ICRF antenna coupling dependence on edge plasma conditions in ASDEX Upgrade

2006 Nucl. Fusion 46 S469

(http://iopscience.iop.org/0029-5515/46/7/S09)

INSTITUTE OF PHYSICS PUBLISHING and INTERNATIONAL ATOMIC ENERGY AGENCY NUCLEAR FUSION

Nucl. Fusion **46** (2006) S469–S475 doi:10.1088/0029-5515/46/7/S09

ICRF antenna coupling dependence on edge plasma conditions in ASDEX Upgrade

Vl.V. Bobkov[1], R. Bilato[1], F. Braun[1], R. Dux[1], J.-M. Noterdaeme[1,2], the ICRF team and the ASDEX Upgrade team

[1] MPI für Plasmaphysik, Boltzmannstr. 2, D-85748 Garching, Germany
[2] Universiteit Gent, EESA Department, B-9000 Gent, Belgium

E-mail: Volodymyr.Bobkov@ipp.mpg.de

Received 5 October 2005, accepted for publication 30 May 2006
Published 21 June 2006
Online at stacks.iop.org/NF/46/S469

Abstract
The relative impact of edge localized modes (ELM) size and plasma shape on the antenna coupling in ASDEX Upgrade discharges is studied. A strong dependence of relative change in the ion cyclotron range of frequencies antenna coupling during ELMs on the ELM size is observed. The changes in the coupling also show some dependence on the plasma triangularity; the latter generally influences the ELM size. At high plasma density and small antenna–plasma distance, however, there is a strong residual correlation of the antenna coupling on the plasma triangularity which appears not to be connected with the ELM size. A possible explanation of this correlation is given in terms of the connection lengths of the magnetic field lines at the antenna. This hypothesis is substantiated by the investigation of L-mode discharges, which are better diagnosed than the ELM phases of the H-mode ones.

PACS numbers: 52.40.Fd, 52.50.Qt, 52.40.Hf

(Some figures in this article are in colour only in the electronic version)

1. Introduction

Radio frequency (RF) heating in the ion cyclotron range of frequencies (ICRF) is an important tool for generating fast ions [1, 2], which are necessary for accessing the physics of energetic alpha particles, so crucial for the transport and stability in ITER and fusion reactor plasmas [3]. The amount and the energy of ICRF-produced fast particles depend critically on the RF power that can be delivered to the plasma and thus on the ICRF antenna coupling efficiency. We study the ICRF antenna coupling in ASDEX-Upgrade L-mode and H-mode discharges for the minority ion heating scheme (hydrogen in deuterium plasmas). In H-mode discharges the appearance of periodic MHD instabilities at the plasma edge with high toroidal mode number, known as edge localized modes (ELM) [4, 5], is accompanied by an abrupt change in the antenna coupling [6].

During these events considerable amounts of plasma particles and energy are expelled and, consequently, the edge plasma density and temperature profiles are greatly affected [7–11]. In the first 200–300 μs of type-I ELMs [4, 5], the largest of ELM perturbations in ASDEX Upgrade [8–12], filamentary-like structures of density appear at the low field side elongated along the magnetic field lines and with characteristic poloidal extent of 5 to 10 cm. These filaments containing relatively dense and hot plasma are then accelerated radially outwards into the scrape-off-layer (SOL). After this relatively short phase with enhanced perpendicular particle and heat transport [7, 11], it takes some milliseconds for the plasma density and temperature profiles to recover.

The largest changes in the antenna coupling among all ELM-like instabilities are observed during type-I ELMs in highly triangular plasmas. These events should, therefore, be studied in order to prepare ICRF systems in future devices to withstand critical coupling variations. The influence of ELMs on the antenna coupling is mainly through the changes in the density profile in the plasma edge. The importance of the density profile close to the launcher follows immediately from the cold-plasma dispersion relation of the launched fast waves (FW) [13]:

$$n_\perp^2 = -\frac{(n_\parallel^2 - \mathcal{R})(n_\parallel^2 - \mathcal{L})}{n_\parallel^2 - \mathcal{S}} \qquad (1)$$

(with $n_\perp$ and $n_\parallel$ the components of the wave index vector perpendicular and parallel to the local confining magnetic field

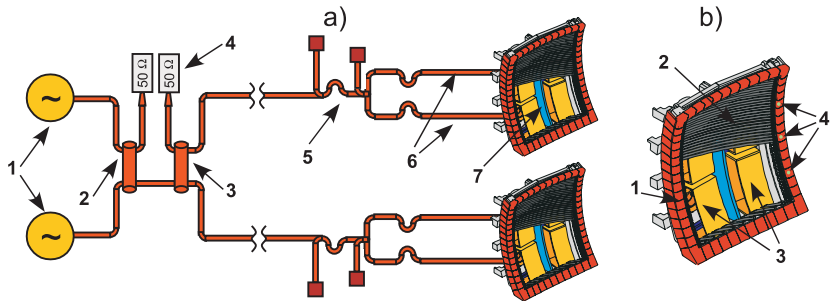

Figure 1. (*a*) One of two double ICRF systems at ASDEX Upgrade; 1—RF generators, 2 and 3—3 dB combiner and splitter, 4—dummy loads, 5—matching network, 6—resonant antenna transmission lines, 7—antenna. (*b*) Double strap ICRF antenna; 1—limiter, 2—Faraday shield, 3—straps, 4—points of observation of a spectroscopic diagnostic.

and the standard notations [13, 14]). Since the launched FW is propagating when $\mathcal{R} > n_\parallel^2$ and $\mathcal{R}$ is proportional to the electron density n_e, the waves propagating from the antenna towards the plasma centre have to tunnel through an evanescence layer of low plasma density $n_e < n_e^{\mathrm{cutoff}}(n_\parallel)$. In turn, the width of the evanescent layer influences the amount of the power transfered to the plasma and thus the antenna resistance. If we use the filtering factor as proposed in [15], we can write for the effective antenna coupling resistance R_{ant}:

$$R_{\mathrm{ant}} \propto \mathrm{e}^{-1.1\, k_\parallel\, d} \tag{2}$$

with d being the width of the evanescence layer and $k_\parallel = n_\parallel \omega/c$ where ω is 2π times the generator frequency. The density at the plasma edge plays an important role also for parasitic power absorption: the presence of high parallel electric fields and not negligible plasma density close to the antenna causes power dissipation in RF sheaths [16]. It has been experimentally observed that the power dissipated in RF sheaths increases with the local plasma density [17–19]. However, in studies of the coupling based on the antenna loading we count this parasitically dissipated power to be coupled power, since it cannot be easily separated from the power effectively delivered to the plasma.

In this paper we study empirically the relative impact of ELM size and plasma shape on the antenna coupling in ASDEX Upgrade discharges.

In section 3 we investigate the influence of the ELM size on the antenna coupling for a dataset ASDEX-Upgrade H-mode discharges with type-I ELMs. As one might expect, we find that the coupling variations increase with ELM size, consistently with the experimental observation that the particle losses increase with ELM size [7, 20]. It is experimentally established [20] and understood ([21] and references therein) that the size and thus the frequency of ELMs depend on the plasma shape, in particular, on the plasma triangularity: the higher the plasma triangularity, the smaller the repetition rate and the larger the size of ELMs. However, as discussed in section 3 the available dataset under consideration shows a residual dependence on the changes in the antenna coupling on the plasma shape (triangularity) not connected with ELM size.

The influence of the plasma geometry on ICRF antenna coupling has been already observed in various devices [22–24]. In particular, both on JET [23] and on ASDEX Upgrade [24] an increase in changes of the coupling has been observed during ELMs for high triangular discharges, which are ITER-relevant for their high H-mode performance. Thus for the design of ITER antennas, it is of great relevance to understand the origin of this sensitivity to the plasma triangularity.

One possible source of this sensitivity can be related to the magnetic field line geometry between the limiter and the ICRF antenna (i.e. in the limiter shadow). Here the local plasma density can be influenced by variations in the lengths of the local magnetic field lines. To shed more light on this possible explanation, we devote the last part of this paper to studying the influence of the plasma geometry on the antenna coupling in L-mode discharges. The choice of the L-mode discharges is useful because it allows more reliable measurements of the edge plasma density profiles and control on edge plasma parameters, such as density at the separatrix for a variety of plasma triangularities. In connection with pure geometrical effects, the analysis done for L-mode discharges helps the understanding of the antenna coupling during ELM phases of the H-mode discharge.

2. ICRF system at ASDEX Upgrade

The ICRF system at ASDEX Upgrade consists of two double systems: as shown in figure 1(*a*), the RF power from two RF generators (1) is combined via a 3 dB combiner (2) to a single line and split into two lines by a 3 dB splitter (3). This configuration [25–27] allows for a good insulation of the RF generators from the reflected power during type-I ELMs by shunting the reflected power into a dummy load (4), if magnitude and phase of the powers reflected from the two antennas are close to each other. A matching network (5) [28] consisting of two stubs is situated at a T-connection of the two antenna resonant lines (6) connected to the double strap antenna (7) located at the low field side of the ASDEX Upgrade tokamak [29].

Each antenna (figure 1(*b*)) includes graphite limiters (1), a Faraday screen (2) and two straps (3). The Faraday screen rods have a 15° inclination with respect to the horizontal plane.

The antenna resistance is derived from the measurements of the forward and reflected RF powers for a single antenna and voltages on both straps. Assuming that the power is equally divided between the two straps, the coupling resistances for each strap is derived. The antenna resistance R_{ant} used in the analysis is an average of two straps.

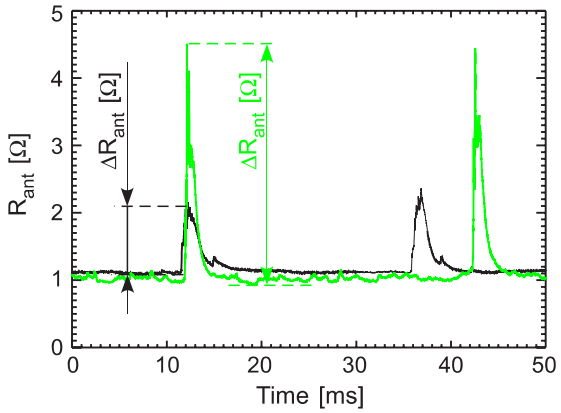

Figure 2. Definition of ΔR_{ant} Black—low triangularity ($\delta_L = 0.28$) and ELM size $\Delta W_{MHD} = 17$ kJ, green—high triangularity ($\delta_L = 0.43$) and ELM size $\Delta W_{MHD} = 22$ kJ.

3. Antenna coupling resistance versus ELM size and triangularity

In this section we examine a set of 75 type-I ELMy H-mode discharges in ASDEX-Upgrade, for a total number of 6730 ELM events. These discharges are characterized by a toroidal magnetic field ranging from 1.9 to 2.1 T and by $f_{ICRF} = 30.0$ MHz with the total RF power varying from 1.5 to 3.5 MW. These parameters fit a minority heating scenario of hydrogen in deuterium, with the hydrogen concentration between 4% and 12%. In this range of concentrations, the theoretical calculations for ASDEX Upgrade show that the minority heating dominates the single pass absorption and that ICRF heating efficiency can be considered as weakly affected by the concentration.

To quantify the ELM size we consider the variation of the plasma stored energy W_{MHD}, determined from the MHD equilibrium reconstruction. Concerning the triangularity, for consistency with the previous analysis [23, 24] we consider the values of the lower triangular parameter δ_L, estimated between two successive ELM events. The variations of both W_{MHD} and the coupling resistance R_{ant} are calculated as the difference between the maximal value during ELM and minimum value between two ELMs, as sketched in figure 2. We further characterize the discharges by two parameters relevant [17, 30] to ICRF coupling: the line averaged density, the density averaged along the central horizontal sight line of the DCN interferometer, and the separatrix–antenna distance. The latter is the minimum distance between the separatrix and the antenna.

Figure 2 shows the time traces of ΔR_{ant} corresponding to two different values of δ_L. As δ_L increases from $\delta_L = 0.28$ to $\delta_L = 0.43$, ELMs become larger (ΔW_{MHD} increases) and increasing values of ΔR_{ant} are observed. The connection between ELM size and antenna coupling changes is confirmed by figure 3 which shows ΔR_{ant} versus ΔW_{MHD} for the ELM event dataset in exam. To highlight the density dependence of ΔR_{ant}, the data set is divided into two subsets, namely, high density $7.5 \cdot 10^{19} < \bar{n}_e < 9.0 \cdot 10^{19}$ m^{-3} in frame (*a*) and low density $5.0 \cdot 10^{19} < \bar{n}_e < 6.5 \cdot 10^{19}$ in frame (*b*). In each of these two graphs, the data is divided into two other subsets—below 3.8 cm or above 4.3 cm of minimum distance between the antenna and separatrix chosen so that the cases of small and large antenna–separatrix distances are isolated and have sufficient number of points. As will be described in the following, the data have been selected to have the average values of safety factor at the plasma edge q_{95} (the ratio of toroidal to poloidal magnetic field components at the magnetic surface corresponding to 95% of flux) as close as possible, i.e. for each subset $\bar{q}_{95} = 4.1 \pm 0.15$.

From figure 3 and the ELM size dependence on δ_L [31], one might conclude that the plasma geometry influence on the antenna coupling observed previously in JET [23] and in ASDEX Upgrade [24] is only an indirect effect due to the ELM size dependence on δ_L. To address this δ_L dependence we evaluate the Kendall's correlation coefficients [32] $\tau(\Delta R_{ant}, \delta_L)$ and $\tau(\Delta R_{ant}, \Delta W_{MHD})$, as shown by the solid bars in figure 4. In addition, we show by hatched bars the correlation between ΔW_{MHD} and δ_L. The main features of figure 4 are (*a*) a higher $\tau(\Delta R_{ant}, \Delta W_{MHD})$ than $\tau(\Delta R_{ant}, \delta_L)$ everywhere except in the high density case with small antenna–separatrix distances where they are comparable and (*b*) an increase in $\tau(\Delta R_{ant}, \delta_L)$ with respect to $\tau(\Delta R_{ant}, \Delta W_{MHD})$ going from lower to higher densities or/and from larger to smaller antenna–separatrix distances. With regard to the correlation between ΔR_{ant} and δ_L, $\tau(\Delta R_{ant}, \delta_L)$ is larger than $\tau(\delta_L, \Delta W_{MHD})$ everywhere except at low densities and large distances. The difference between these two coefficients becomes larger for smaller distances and for higher densities. Thus ΔR_{ant} is better correlated with δ_L than expected only via its relation with ΔW_{MHD} (except at low densities and large distances). Consequently, part of the ΔR_{ant} dependence on δ_L is probably due to other mechanisms which are not directly connected with ΔW_{MHD} and which influence the edge plasma density.

A reasonable candidate responsible for this 'residual' plasma shape dependence can be sought in the connection lengths of the magnetic field lines just in front of the ICRF antenna. This should be more evident at higher densities when the cut-off density location shifts closer to the antenna and the vessel/antenna structures become more important.

The connection lengths of the field lines in the far SOL depend on the magnetic field inclination angles near vessel structures. The angles, i.e. local ratios between the poloidal and the toroidal magnetic field lines, are well defined by the plasma shape and values of q_{95}. In the poloidal plane (e.g. see below in figure 5), it appears that generally the plasma shapes with lower values of the plasma triangularity δ_L have the magnetic flux surface fitting significantly better to the contour of the ICRF antenna limiter (please refer to section 4 to see that a better fit of the shape to the limiter leads to smaller connection lengths). If q_{95} is kept constant, one can take δ_L as the only important parameter for connection lengths in front of the ICRF antenna.

As a matter of fact, the distribution of q_{95} values in our dataset is discrete and does not allow for a similar correlation analysis as done for δ_L or ΔW_{MHD}. Analysis of isolated cases with q_{95} in very narrow ranges confirms the picture described above on the basis of figure 4 and does not interfere with the conclusions.

In the next section we address the effect of the connection length of the magnetic field lines by examining two L-mode

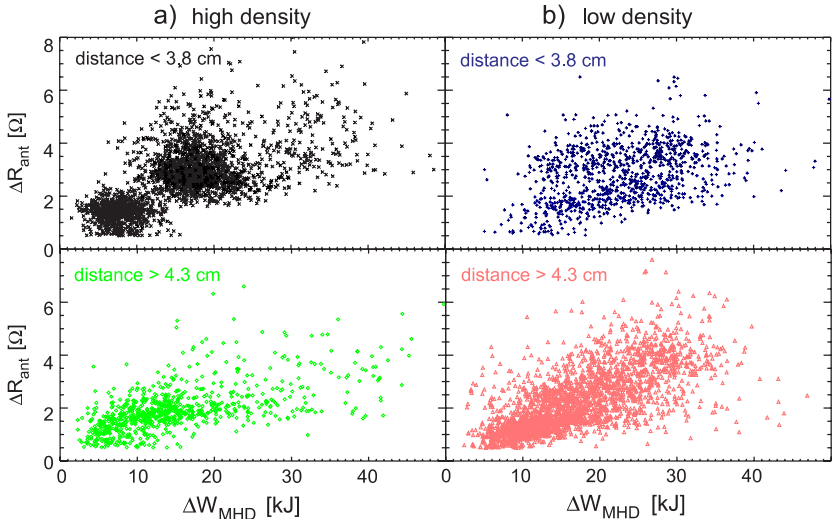

Figure 3. Change in antenna resistance $\Delta R_{\rm ant}$ versus loss of stored plasma energy during an ELM $\Delta W_{\rm MHD}$. (*a*) Line averaged densities $7.5 \cdot 10^{19} < \bar{n}_{\rm e} < 9.0 \cdot 10^{19}\,{\rm m}^{-3}$ (×, upper graph)—minimum antenna–separatrix distance <3.8 cm, (◊, lower graph)—minimum antenna–separatrix distance >4.3 cm. (*b*) Densities $5.0 \cdot 10^{19} < \bar{n}_{\rm e} < 6.5 \cdot 10^{19}\,{\rm m}^{-3}$, (+, upper graph)—minimum antenna—separatrix distance <3.8 cm, (△, lower graph)—minimum antenna–separatrix distance >4.3 cm.

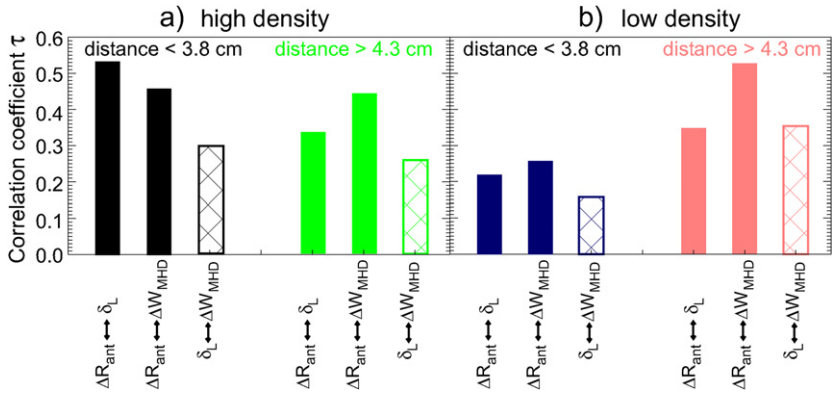

Figure 4. Three correlation coefficients $\tau(\Delta R_{\rm ant}, \delta_{\rm L})$, $\tau(\Delta R_{\rm ant}, \Delta W_{\rm MHD})$ and $\tau(\delta_{\rm L}, \Delta W_{\rm MHD})$ for each set of data. (*a*) Line averaged densities $7.5 \cdot 10^{19} < \bar{n}_{\rm e} < 9.0 \cdot 10^{19}\,{\rm m}^{-3}$, dark bars—antenna–separatrix distance <3.8 cm, light bars—antenna–separatrix distance >4.3 cm. (*b*) Densities $5.0 \cdot 10^{19} < \bar{n}_{\rm e} < 6.5 \cdot 10^{19}\,{\rm m}^{-3}$, dark bars—antenna–separatrix distance <3.8 cm, light bars—antenna–separatrix distance >4.3 cm.

discharges at two different triangularities and about the same magnetic field inclination angle at the edge. The L-mode discharges fit better the purposes of the following analysis since the geometrical effects linked to the connection lengths of the magnetic field lines cannot be always singled out during the abrupt expulsion of particles in the ELM phase. In addition, for a consistent analysis it is mandatory to measure the change in the density profile in front of the antenna and this is problematic during ELM phases.

4. Antenna coupling resistance versus shape of magnetic field lines: L-mode

The two L-mode discharges with different shapes reported in figure 5 are discharge #19795 with $\delta_{\rm L} = 0.27$ and $q_{95} = 4.7$ and discharge #19793 with $\delta_{\rm L} = 0.41$ and $q_{95} = 5.3$. The plasma shape of $\delta_{\rm L} = 0.27$ discharge fits better the contour of the ICRF antenna limiter than that of the $\delta_{\rm L} = 0.41$ one. Both discharges have a toroidal magnetic field of 2.5 T and the inclination of magnetic field lines with respect to the horizontal plane at the antenna is 8.8° and 7°, respectively.

The line averaged density is $4.4 \cdot 10^{19}\,{\rm m}^{-3}$ in both discharges and deuterium was puffed in as working gas. Finally, in both discharges the ICRF power coupled at 36.5 MHz is 1.5 MW, just below the L–H threshold [33].

Figure 6 shows the coupling resistance $R_{\rm ant}$ during a scan of the radial position of the plasma column: in frame (*a*) $R_{\rm ant}$ is plotted versus the minimum antenna–separatrix distance, whereas in figure 6(*b*) it is plotted versus the average distance antenna–separatrix, calculated by integrating the distance between the separatrix and the antenna limiter along the vertical antenna extension. When the measured $R_{\rm ant}$ is plotted as function of the minimum plasma distance, the $\delta_{\rm L} = 0.27$ appear to be close to the curve of $\delta_{\rm L} = 0.41$ values (figure 6(*a*)). However, when plotted as a function of the average distance (figure 6(*b*)), the $R_{\rm ant}$ values locate at two different levels, higher values for higher triangularity. A similar behaviour has been observed also in JET where antenna coupling in L-mode discharges of different plasma shapes was

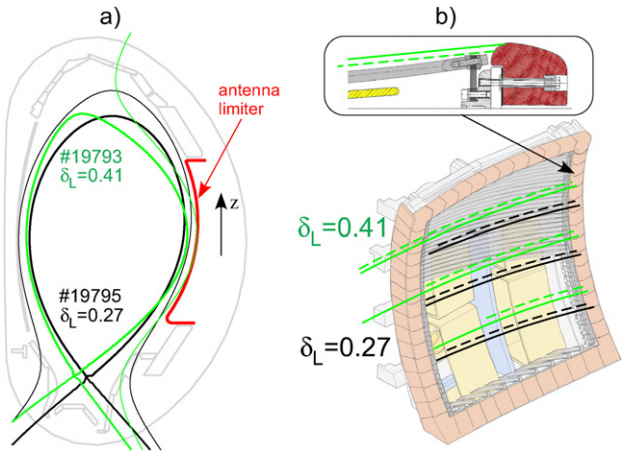

Figure 5. (*a*) Two discharge shapes: black—$\delta_L = 0.27$ (plasma shape matches well the contour of ICRF antenna limiter), green—$\delta_L = 0.41$. Thin lines present FW cut-off surfaces derived with the help of density profiles in figure 7. (*b*) Magnetic field line geometry, solid lines start on the limiter edge close to plasma, dashed lines start on the limiter in its shadow far from plasma (as shown at the top); $\delta_L = 0.27$—black, $\delta_L = 0.41$—green.

analysed [34]. An empirical fit of the antenna resistance was made for three distances between the separatrix and antenna: near the top, the middle and the bottom of the antenna. The fit shows that the influence of the antenna–plasma distances at the top and at the bottom is about 15 times smaller than the influence of the middle distance. The middle distance for all shapes used in [34] was very close to the minimum separatrix–antenna distance.

For the two discharges under consideration, figure 7 shows the electron density profiles (mapped to the mid plane) provided by Thomson scattering diagnostics which measures the densities at the plasma edge [35, 36]. These profiles are measured during the radial movement of the plasma and the fitting solid lines are obtained with a Bayesian filter [37]. The FW cut-off density for the dominant $k_\parallel$-component of the ICRF antenna spectrum ($k_\parallel = 7.55\,\mathrm{m}^{-1}$ for 0π antenna phasing) is approximately $3.8 \cdot 10^{18}\,\mathrm{m}^{-3}$ (horizontal line in figure 7). Since the discharge with higher δ_L has a flatter and higher density profile in the SOL, the width of the evanescence layer for the launched FW is smaller than in the $\delta_L = 0.27$ case (see cut-off surfaces in figure 5(*a*)), and, consequently, the antenna coupling is better, in agreement with what is observed in figure 6(*b*).

Using as weight function the filtering factor proposed in [15] (equation (15)), which takes into account the optical thickness of the evanescence layer as a function of the distance g(z), we define an effective antenna–separatrix distance:

$$g_{\mathrm{eff}} = \frac{1}{z_{\mathrm{up}} - z_{\mathrm{down}}} \int_{z_{\mathrm{down}}}^{z_{\mathrm{up}}} g(z)\, \mathrm{e}^{-1.1\, k_\parallel\, (g(z) - g_{\mathrm{min}})}\, \mathrm{d}z. \qquad (3)$$

Figure 8 shows the R_{ant} values for the two discharges as a function of g_{eff}. The two sets of R_{ant} values are different because of the difference in the cut-off locations with respect to the separatrix. For an estimate, we assume that this difference $\Delta g_{\mathrm{cutoff}}$ is approximately the same over the plasma contour near the antenna and $\Delta g_{\mathrm{cutoff}} \approx 2$ cm from figure 8. A factor of $\exp(1.1 k_\parallel \Delta g_{\mathrm{cutoff}}) \approx 1.2$ is obtained as the difference between the two sets of R_{ant} values. This confirms that the main difference between the two discharges can be explained on the basis of the different density profile in front of the antenna, as measured by the Thomson scattering diagnostics.

We consider the longer connection lengths in the SOL and in particular in the limiter shadow as one of the main reasons for the higher SOL plasma density for the higher triangular discharge. Figure 5(*b*) shows the magnetic field line geometry in three poloidal positions at the antenna surface. The field lines, which in the limiter shadow do not hit the neighbouring structures (solid lines), have a longer connection length for higher triangularity. If one considers the balance between the loss along and the loss across the field line, the longer connection lengths should collect higher densities. In agreement with this assumption, the SOL density profile has an e-folding length which increases with the connection length [38].

However, the difference in the connection lengths alone can hardly explain the difference in the density profiles measured at the plasma edge outside the limiter shadow. Another effect is that due to the longer connection lengths a stronger plasma–wall interaction and subsequent gas ionization takes place in the case of the high triangularity discharge and which in turn leads to the higher density also far from the antennas. There are at least two pieces of experimental evidence that corroborate this picture. To maintain the line average density of about $4.4 \cdot 10^{19}\,\mathrm{m}^{-3}$ for both discharges a deuterium gas puff via the mid plane gas valves at the low field side was used, at marginally higher ($\approx$10%) rate for the lower triangularity discharge. Although no hydrogen was puffed, the concentration of hydrogen was significantly lower for lower triangularity, namely 6.5% for $\delta_L = 0.27$ and 12% for $\delta_L = 0.41$ according to the charge-exchange measurements [39]. This suggests a the stronger plasma-wall (and possibly plasma-antenna) interaction for the higher triangularity case, where significant particle fluxes can hit more remote vessel structures and release hydrogen which was stored in the walls. Depending on the differences in the particle influxes, differences in the recycling processes can play a significant role. This is also confirmed by the measured neutral gas flux in the main chamber, which is a factor of two higher for the discharge with $\delta_L = 0.41$. In fact for this discharge the inner-divertor strike point does not fit in the well-baffled region of the divertor, where the neutral gas flux is a factor of two lower compared with the shape with $\delta_L = 0.27$. As a consequence, in the high triangularity shape the neutral gas balance is shifted to the main chamber which participates in recycling processes more extensively. It is worthy of note that H-modes show essentially the same tendency of the neutral gas flux balance at high triangularity [31].

According to these experimental observations, it is natural to expect significant changes of the antenna coupling during variations of the shape of the magnetic field lines in the SOL. Thus in H-mode ELMs may lead to a more intense antenna–plasma interaction for the cases of high triangular discharges and cause higher changes in the antenna coupling.

The dependence of the antenna coupling on the magnetic field geometry has been also observed in the limiter configuration on Tore Supra [22], where the geometry is changed, e.g. by switching first the limiting surface between

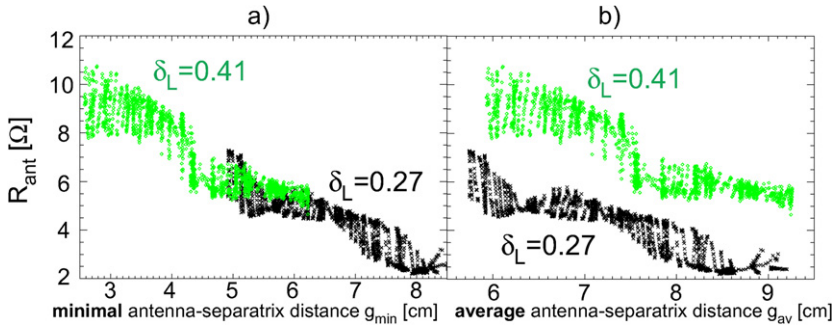

Figure 6. Antenna resistance, black for $\delta_L = 0.27$ and green for $\delta_L = 0.41$ versus (*a*) minimum antenna–separatrix distance and (*b*) average antenna–separatrix distance integrated along *z*-axis from figure 5(*a*) (vertical antenna extension).

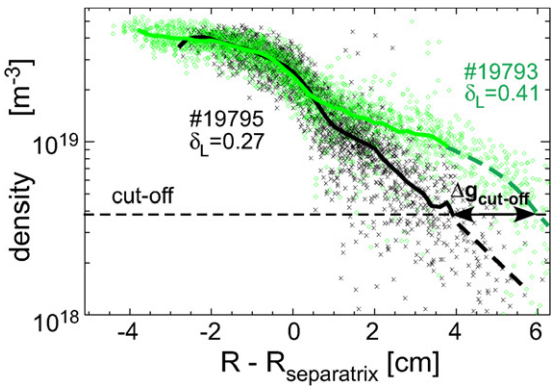

Figure 7. Density profiles for discharges with $\delta_L = 0.27$ (△, black) and $\delta_L = 0.41$ (×, green). Curves—data filtered with Bayesian filter [37].

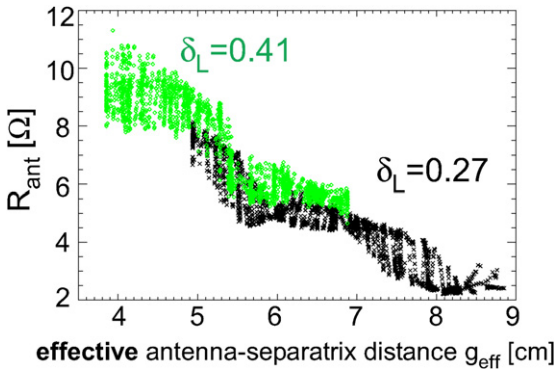

Figure 8. Antenna resistance, black for $\delta_L = 0.27$ and green for $\delta_L = 0.41$ versus effective antenna–separatrix distance integrated along the z-axis from figure 5(*a*) (vertical antenna extension) according to equation (3).

the inner wall and the outer wall with the outboard pumped limiters.

Modelling of the ICRF influence on plasma density [40–42] is required to improve the understanding of the processes of plasma-antenna interaction for different discharge geometries.

5. Conclusions

The coupling resistance R_{ant} of the ASDEX-Upgrade ICRF antennas during type-I ELMs depends strongly on the ELM size, but correlates also with the plasma geometry. The particle losses during ELM events govern the density profile at the plasma edge and, consequently, the antenna coupling performance. The higher the ELM size is, the higher the coupling variations are. There is, however, a dependence of the changes of the antenna coupling on the plasma shape which is not directly related with the ELM size. This is more evident at relatively high plasma densities and small antenna–plasma distances. In these situations, variations of the triangularity affect gas recycling (and thus the edge plasma density) through the change of the connection lengths of magnetic field lines in the scrape-off layer. This effect has been investigated in well-diagnosed L-mode discharges.

A reliable extrapolation to ITER will be possible only with further experimental investigation of the ICRF coupling and its modelling with a self-consistent evaluation of the ICRF influence on the density.

Acknowledgments

We would like to thank Drs O. Gruber, J. Neuhauser, I. Monakhov and M.-L. Mayoral for valuable discussions. We are also indebted to Dr M. Brambilla for the comments and reading of the manuscript.

References

[1] Putvinski S.V. 1998 *Nucl. Fusion* **38** 1275
[2] Mantsinen *et al* 2005 *Plasma Phys. Control. Fusion* **47** 1439–57
[3] ITER Physics Expert Group on Energetic Particles Heating and current drive and ITER physics basis editors 1999 *Nucl. Fusion* **39** 2471
[4] Zohm H. 1996 *Plasma Phys. Control. Fusion* **38** 105–28
[5] Connor J.W. 1998 *Plasma Phys. Control. Fusion* **40** 531–42
[6] Noterdaeme J.-M. *et al 21th EPS Conf. on Plasma Physics and Controlled Fusion* (*Montpellier, 1994*) ECA vol 18B pp 842–45
[7] Loarte A. *et al* 2003 *Plasma Phys. Control. Fusion* **45** 1549–69
[8] Herrmann A. *et al Proc. 20th Int. Conf. on Fusion Energy 2004 (Vilamoura, Portugal, 2004)* (Vienna: IAEA) CD-ROM file EX/2-4Rb and http://www-naweb.iaea.org/napc/physics/fec/fec2004/datasets/index.html
[9] Kirk A. *et al* 2005 *Plasma Phys. Control. Fusion* **47** 995–1013
[10] Horton L.D. *et al* 2005 *Nucl. Fusion* **45** 856–62
[11] Leonard A.W. *et al* 2001 *J. Nucl. Mater.* **290–293** 1097–101
[12] Eich T. *et al* 2003 *Phys. Rev. Lett.* **91** 195003
[13] Stix T. 1992 *Waves in Plasmas* (New York: American Institute of Physics)

[14] Brambilla M. 1998 *Kinetic Theory of Plasma Waves* (Oxford: Oxford Science Publications/Clarendon)
[15] Bilato R., Brambilla M., Hartmann D.A. and Parisot A. 2005 *Nucl. Fusion* **45** L5–7
[16] Myra J.R. *et al* 2005 *16th Topical Int. Conf. on Radio Frequency Power in Plasma (Park City, USA) AIP Conf. Proc.* **787** 3–14
[17] Colas L. *et al* 2003 *Nucl. Fusion* **43** 1–15
[18] Bobkov Vl.V. *et al* 2003 *J. Nucl. Mater.* **313** 956–61
[19] Bobkov Vl.V. *et al* 2003 *30th EPS Conf. on Plasma Physics and Controlled Fusion (St. Petersburg, Russia)* ECA vol 27A P-1.165
[20] Urano H. *et al* 2003 *Plasma Phys. Control. Fusion* **45** 1571
[21] Snyder P.B. and Wilson H.R. 2003 *Plasma Phys. Control. Fusion* **45** 1671
[22] Goniche M., Brémond S. and Colas L. 2003 *Nucl. Fusion* **43** 92–106
[23] Monakhov I. *et al* 2003 *15th Topical Int. Conf. on Radio Frequency Power in Plasma (Moran, USA) AIP Conf. Proc.* **694** 146–9
[24] Bobkov Vl.V. *et al* 2005 *J. Nucl. Mater.* **337** 776–80
[25] Goulding R.H. *et al* 1995 *11th Topical Int. Conf. on Radio Frequency Power in Plasma (Palm Springs) AIP Conf. Proc.* **355** 395–400
[26] Braun F., Hofmeister F., Wesner F., Becker W., Faugel H., Hartmann D. and Noterdaeme J.-M. 2001 *Fusion Eng. Des.* **56** 551–5
[27] Noterdaeme J.-M. *et al* 1997 *Proc. 16th Int. Conf. on Fusion Energy 1996 (Montreal, Canada, 1996)* (Vienna: IAEA) **3** 335–42
[28] Hofmeister F. Braun F. and Wesner F. 1994 *Fusion Eng. Des.* **24** 83–9
[29] Noterdaeme J.-M. *et al* 1994 *Fusion Eng. Des.* **24** 65–74
[30] Hartmann D.A. *et al* 2001 *14th Topical Int. Conf. on Radio Frequency Power in Plasma (Oxnard, CA, USA) AIP Conf. Proc.* **595** 130
[31] Suttrop *et al* 2000 *Plasma Phys. Control. Fusion* **42** A97–102
[32] Snedecor G.W. and Cochran W.G. 1989 *Statistical Methods* 8th edn (Ames, Iowa: Iowa State University Press) pp 177–95
[33] Ryter F. *et al* 1998 *Plasma Phys. Control. Fusion* **40** 725
[34] Bilato R. *et al* 2004 *31th EPS Conf. on Plasma Physics and Controlled Fusion (London, UK)* (ECA) vol 28G P-5.164
[35] Murmann H. *et al* 1992 *Rev. Sci. Instrum.* **63** 4941–3
[36] Kurzan B. *et al* 2001 *Rev. Sci. Instrum.* **72** 1111–4
[37] Dose V.T. 2001 *Nucl. Fusion* **41** 1671
[38] Wesson J. 2004 *Tokamaks 3rd edn* (Oxford: Clarendon) 449–53
[39] Fahrbach H.-U., Max-Planck-Institute for Plasmaphysics 2005 Private communication
[40] Clairet F., Colas L., Heuraux S. and Lombard G. 2004 *Plasma Phys. Control. Fusion* **46** 1567–80
[41] Colas L. *et al* 2005 *16th Topical Int. Conf. on Radio Frequency Power in Plasma (Park City, USA) AIP Conf. Proc.* **787** 150–7
[42] D'Ippolito D.A. *et al* 2005 *16th Topical Int. Conf. on Radio Frequency Power in Plasma (Park City, USA) AIP Conf. Proc.* **787** 222–5